JOURNAL OF MATERIALS SCIENCE 25 (1990) 4440–4448

In situ laser irradiation of WC–Co hard metals inside a scanning electron microscope

Part 2 *Behaviour of the cobalt binder*

H. MÜLLER, K. WETZIG, B. SCHULTRICH
Akademie der Wissenschaften der DDR, Zentralinstitut für Festkörperphysik und Werkstofforschung, Helmholtzstr. 20, DDR-8027 Dresden, GDR

S. M. PIMENOV, N. I. CHAPLIEV, V. I. KONOV, A. M. PROCHOROV
Institute of General Physics, Academy of Science of the USSR Vavilova street 38, 117 333 Moscow, USSR

Cemented carbides with higher binder contents were irradiated with a CO_2-pulse laser within a SEM to investigate the structural development in more detail. The decisive medium is the melting binder which dissolves the refractory carbide phase. In this way a superficial layer of an oversaturated solid solution with highly dispersed secondary carbides is produced. At higher pulse numbers a periodic structure is engraved in the surface by local evaporation as result of a self-amplifying resonance phenomenon.

1. Introduction

Part 1 [1] of this work was dealing with general features of laser surface modification of WC–Co hard metals investigated inside a scanning electron microscope (SEM). Samples with 6 wt % Co binder and different surface states (as-received from sintering, ground and mechanically polished) were studied. Based on the analysed irradiation conditions (reflection coefficient of the polished sample, pulse energy, temporal and spatial pulse shape) an approximated calculation of the temperature field was given. The maximum surface temperature of about 2100° C was higher than the melting temperature of the cobalt binder phase (T_m = 1350° C) but below the melting point of WC (T_m = 2700° C). This suggests a certain relationship to the processes in liquid phase sintering which uses the lower melting binder for densification of the refractory phase. Powder metallurgical production of these materials involves the following stages of sintering [2]: (1) Partial dissolution of tungsten and carbon in cobalt in the solid state between 1000 and 1350° C; (2) lowering of the melting point of the cobalt phase (from 1450° C to about 1350° C) by substitutional and interstitial alloying; (3) melting of the cobalt alloy at 1350° C; (4) intense solution and reprecipitation of the solved components as WC due to the temperature-dependent solubility.

The investigation presented in Part 1 supported the statement that structural modifications by laser processing and by liquid phase sintering are based on the same mechanism: under irradiation with a maximum surface temperature of about 2100° C the transformation of the surface layer is not caused by direct melting of the carbide phase but by progressive solution of the carbides in the binder melt. Hence the liquid fraction increases, in this way improving the coupling conditions with the laser beam. Due to self-quenching under pulse irradiation the oversaturated solution remains frozen in.

In order to study the role of the cobalt binder in more detail the laser irradiation was performed on WC–Co hard metals with a large binder fraction of 32 vol %. The structural development as a result of successive laser pulses was followed by direct SEM investigation during irradiation as well as by detailed investigation of the final state by the aid of different electron microscopic methods.

2. Experimental conditions

The investigated hard metal was produced along the usual powder metallurgical lines by liquid phase sintering. It contains WC grains of mean crystal size 1 to 2 μm and 20 wt % Co (corresponding to 32 vol %). In this part of our work only polished surfaces (mean surface roughness 0.1 μm) were irradiated inside a scanning electron microscope MREM-100 with a CO_2 laser model 143 under the same conditions as in [1]. The angle of incidence was chosen as 45°. The pulse energy and the maximum power density were 24.2 mJ and 160 MW cm^{-2}, respectively. The pressure inside the sample chamber amounted to about 10^{-6} torr. The CO_2 laser was working in TEM_{00}-mode, polarized perpendicular to the plane of incidence. The measurements of pulse energy, as well as temporal and spatial pulse shape, were discussed previously [1].

Besides the SEM in situ techniques, further experimental methods were applied. The element distribution was investigated by EPMA (Electron Probe Micro-Analysis). Special SEM and TEM replica techniques were used for studying the surface relief. Furthermore, a new ion beam slope cutting technique, developed by Hauffe [3, 4], was applied in order

0022–2461/90 $03.00 + .12

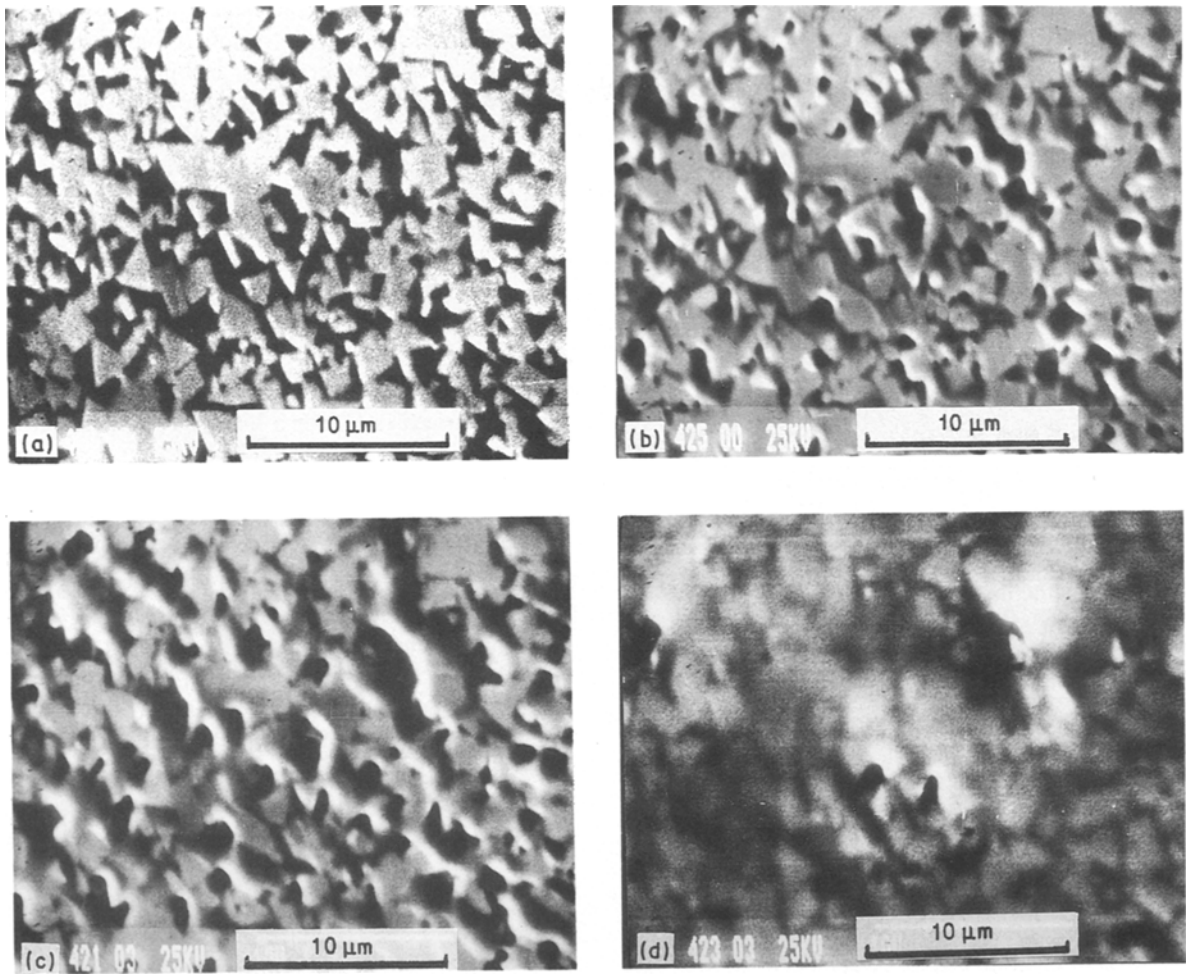

Figure 1 SEM micrograph of a polished surface of a WC–20 wt % Co hard metal, demonstrating the microstructural changes by laser irradiation; (a) initial state, (b) 500 pulses, (c) 1000 pulses, (d) 3000 pulses.

to produce a cross section through a near surface area of the sample: part of the surface is shielded from the tilted (45°) ion beam, which results in a sloping cut. This technique offers the advantage that the slope is free from mechanical deformations. It is smooth, and because of the high sharpness of the produced edge the structural details in the edge region can be seen simultaneously from the original surface and from the cut. Thus a very good impression of the three-dimensional structure of the sample is achieved.

3. Formation of the melt layer

The initial state of the irradiated surface is shown in Fig. 1a. The hexagonal WC grains appear as bright areas and the cobalt binder phase as dark regions between them. With the irradiation conditions used the first laser pulses only led to a surface cleaning, without any surface modifications as it was previously seen on samples with 6 wt % Co [1]. After 50 pulses steps with a bright topographic contrast may be observed at some interfaces between WC grains and the surrounding cobalt binder phase. This topographic image contrast is caused by small binder walls at the WC grains, which appear when molten cobalt binder is starting to creep over the WC grains, because of the excellent wetting of WC by the liquid cobalt binder phase. This process is stopped by resolidification at the end of the laser pulse. With increasing number of laser pulses the number of these walls also increases. They act as starting points for successive creep of the cobalt binder over the WC grains, covering them more and more (compare Fig. 1b and c). Concerning the binder regions, two tendencies are visible in these figures. (1) Due to displacement of binder material towards the carbide grain surfaces, these regions become at first shallow depressions and, finally, deep holes. (2) With increasing fraction of molten material on the surface, these holes are narrowed and the polygonal boundaries change into circular ones. Beginning with the smaller binder regions and the corresponding smaller holes, they are completely eliminated with increasing number of laser pulses. Finally, the spot centre is covered by a continuous nearly pore-free film (see Fig. 1d), whereas the holes are concentrated at the less irradiated margin of the laser spot. In the beginning the layer is very thin, being transparent for the electron beam of 20 kV, which means a thickness of about 0.1 μm or less. The polygonal WC boundaries nearly buried under the drop-like shell of molten material become partially visible again under the even film. These steps in the development of the melt layer are summarized in the scheme given in Fig. 2.

The increasing fraction of material, which is transformed via the liquid state is essentially produced by

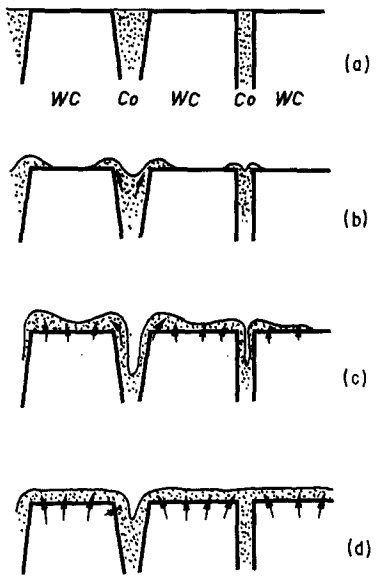

Figure 2 Scheme of the development of the covering melt layer. (a) Section through the WC–Co hard metal with the original polished surface. (b) Start of binder creep over the free carbide surface forming binder walls on the grains and cavities in the binder regions. (c) Complete covering of the surface with a melt layer. (d) Intense carbide dissolution in the melt layer leading to an extended, but flat transformed layer with high WC content.

the progressive dissolution of tungsten carbide in the melt. This essential fact, already stated in [1] shall be discussed in more detail on the basis of the binary section Co–WC of Co–W–C phase diagram (Fig. 3) [5]. A large miscibility gap exists between the fcc Co-rich mixed crystal and the hexagonal α-WC. The solubility of cobalt in tungsten carbide can be neglected. The solubility limit of tungsten in cobalt lies at about 10 at% at the eutectic temperature of 1350° C. It varies strongly with carbon content (in the limiting cases between $\leqslant 1$ at% in equilibrium with graphite and 18 at% for the carbon-free case) [6]. The temperature field in the surface region was calculated with the approximations discussed in [1], especially without considering any phase transformations. However, the latent heat consumed during the melting process does not strongly influence the energy balance. As a conservative estimation the depth h of molten binder can be taken from these calculations as about 1 μm. With the heat of fusion $Q_{Co} = 2.4\,J\,cm^{-3}$ for cobalt and considering the binder volume fraction $f = 0.3$, the latent heat yields the amount $q_{st.en.} fhQ_{Co} = 0.07\,J\,cm^{-2}$ or 3% compared with the total absorbed energy density of $2.2\,J\,cm^{-2}$. Due to the higher binder fraction the absorption coefficient (10%), density ($13.8\,g\,cm^{-3}$), specific heat ($230\,W\,sec\,kg^{-1}\,K^{-1}$) and the thermal conductivity ($60\,W\,K^{-1}\,m^{-1}$) of the hard metal differ from those discussed in [1] for a binder volume fraction of 10%. Although, these changes almost cancel each other out, such that nearly the same temperature distribution is realized, especially the peak temperature on the surface deviates only by some per cent. It is about 2200° C, well above the binder melting point of 1350° C. With the onset of the liquid phase the dissolution of the carbide is very accelerated as it is known from liquid phase sintering. From growth kinetics of the carbide grains during liquid phase sintering of WC-Co via Ostwald-ripening, it was concluded that the dissolution process of WC in liquid cobalt is reaction controlled with an activation energy of $586\,kJ\,mol^{-1}$ [7]. The dissolution rate is approximatively given by [8]

$$dn_W/dt = k(T)[c_0(T) - c]$$

where n_W denotes the number of W-atoms solved in the binder, c is the corresponding concentration $c = n_W/(n_W + n_{Co})$, and $c_0(T)$ is the equilibrium concentration of the melt in contact with WC at temperature T. The time dependence of the surface temperature $T(t)$, of the equilibrium concentration $c_W^0(t)$ and of the rate constant $k(t)$ are represented in Fig. 4 together with an estimation of the resulting mean tungsten concentration $c_W(t)$ in the melt. Due to the very fast temperature change of order $10^{-9}\,K^{-1}$, the tungsten content will remain behind the

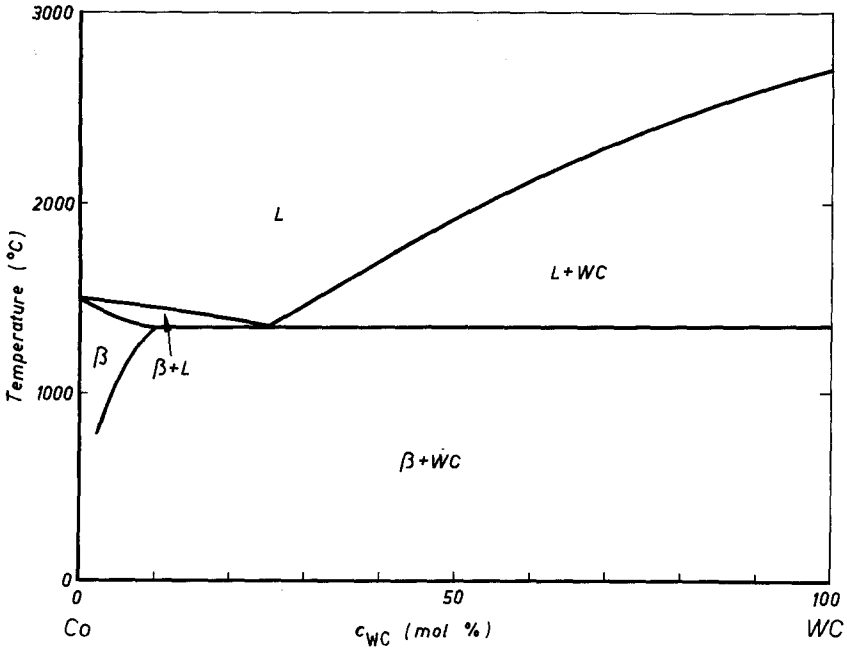

Figure 3 Binary section WC–Co of the Co–W–C phase diagram (after [5]).

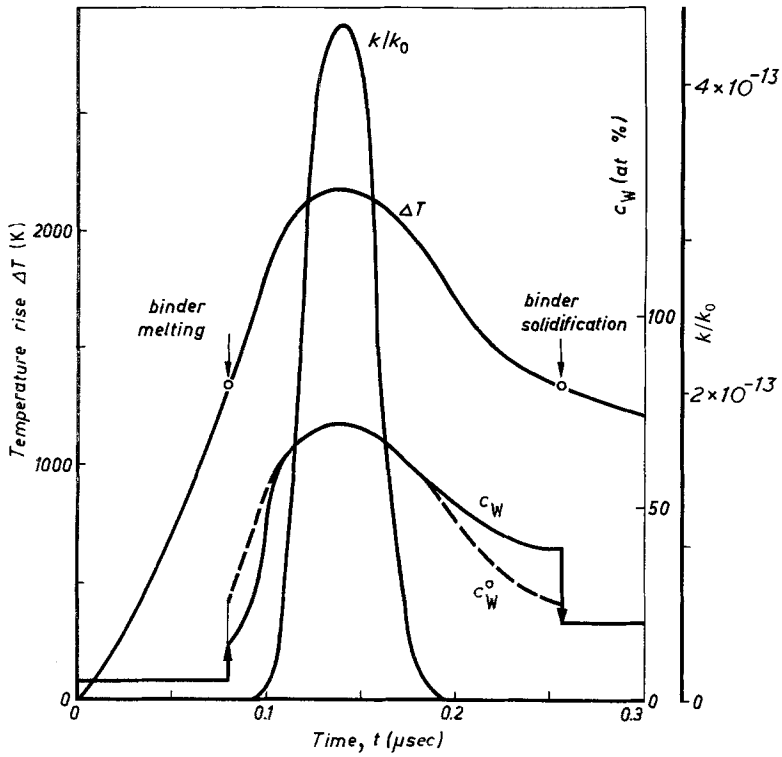

Figure 4 Time dependence of surface temperature $T(t)$, rate constant $k(t)$, equilibrium tungsten concentration $c_W^0(t)$ and real tungsten concentration $c_W(t)$.

equilibrium concentration except for the highest temperatures where the reaction rate is sufficiently high. Hence, an oversaturated solid solution will be solidified at the eutectic temperature together with highly dispersed tungsten carbide grains. These fine crytalline WC precipitates are directly visible by SEM-replica and especially by higher resolving TEM-replica micrographs for WC–Co (Fig. 5). For the next laser pulses this picture must be modified because the fine WC particles have a much larger solution pressure corresponding to replacement of the equilibrium concentration c_0 by $c_0 \exp(2\sigma V_m/rRT)$, where σ denotes the surface tension, r the particle radius and V_m the mole volume. At the same time the rate constant is increased in proportion to the enlarged surface area. These effects stimulate the dissolution process and lead to a rising fraction of material included in the melt. X-ray examination shows that independent of the markedly enlarged melt fraction the ratio of phases with the cobalt and with the WC structure before and after laser irradiation is not much changed. This fact proves the high tungsten and carbon content in the melt, crystallizing to tungsten carbide during cooling.

These processes are furthermore influenced by the rise of the absorption coefficient due to the changing surface state, by transition to the liquid phase and by binder alloying. It this way the absorptance is increased during one pulse by the melt process and with increasing pulse number.

4. Development of periodic structure

The transient existence of a liquid layer causes the development of linear periodic structures with increasing pulse numbers. This can best be seen at lower magnifications where the whole spot may be comprehended (Fig. 6, compare with the detailed illustration in Fig. 2). Between 1000 and 3000 pulses (Fig. 6a,b) the visible spot area, i.e. the region where superficial melting proceeds, extends markedly. The advanced binder film formation after 3000 pulses is accompanied by a weak periodic structure of the film at the border of the spot (Fig. 6b). This structure is aligned perpendicular to the projection of the incident laser beam on the surface. A similar phenomenon was observed for the irradiation with unpolarized light pulses from a neodymium-glass laser for cemented carbides [9] and other materials. Notwithstanding the significant alterations of surface topology in the centre, the structure in the outer regions is not much changed even in the immediate neighbourhood of the periodic ripples, as it can be seen from the invariance of pores and of elements of the primary weak structure (compare Fig. 6b and c). The ripple region lies asymmetrically displaced along the beam direction. It is sharply bounded especially at its back part, but the periodicity continues beyond the spot boundaries as a weakly visible contrast. Continued laser irradiation leads to further extension of the rippled region (Fig. 6d) over the prevailing part of the spot. A thorough comparison shows that the position of the ripples has not changed, which proved the static nature of these patterns. At the same time the destruction of the ordered surface relief by intensified melting (already indicated in Fig. 6c in the irradiation centre) proceeds, transforming the periodic structure to an irregular roughness (Fig. 6e).

The formation of such periodic structures by the action of intense laser light was already observed in the early days of laser investigation [10]. This phenomenon was studied with growing interest from its theoretical foundations and for a series of relatively homogeneous materials as metals, semiconductors and glasses (for a review see [11]). The investigation of these effects in strongly heterogeneous materials as cemented carbides, to our knowledge first represented

in this paper, allows a more detailed investigation of the structural changes leading to the periodic surface modulation by means of the intrinsic small-scaled structural marks.

For understanding of the formation of the regular surface pattern, it is useful to consider the statistical roughness as a superposition of sinusoidal components of different wavelength (corresponding to the spatial Fourier spectrum). The electromagnetic surface wave, which is induced by the incident laser light on the electrically conducting material, is modified by interference of the partial waves scattered from the periodic surface roughness. The resulting amplitude achieves a sharp maximum for in-phase superposition, i.e. if the roughness periodicity fulfills certain resonance conditions. If there exists any kind of positive feedback of field modulation to surface roughness, this resonance mode will be extraordinarily amplified, and in the competition with the other Fourier components it will be selected as the only dominating mode. For such a roughness enlarging mechanism, evaporation processes have been proposed [11].

In the current experiments the laser beam was polarized perpendicularly to the plane of incidence. In this case, for optimum wave enhancement the normal direction of the ripple patterns should be perpendicular to the plane of incidence (parallel to the electrical force) and the distance d of the ripples should satisfy the relation $d = \lambda/\cos\theta$ with θ the angle of incidence [11]. Both conditions are strictly fulfilled for the periodic structure reproduced in Fig. 6 to Fig. 9. The correct orientation is obvious from the orthogonality to the primary weak structure marking the beam direction. The distance d between the ripples follows from Fig. 8 or Fig. 9 as $d = 13\,\mu m$, which is consistent with the theoretical value $d = \lambda/\cos 45° = 15.0\,\mu m$, if the experimental uncertainty of magnification factor and angular adjustment of the sample are considered. (The deviating distance $10\,\mu m$ on the in situ micrographs in Fig. 6 is caused by the projection on the tilted plane of electronmicroscopical image).

On the first view the clearly visible continuation of the periodic pattern outside the molten area seems to be a surprising effect. The cause is the modulated surface wave mentioned above which transmits electromagnetic energy behind the irradiated zone and converts it there into a fluctuating temperature field synchronously with the inducing periodic roughness inside the spot [12, 13]. Fixing and visibleness of these relatively low temperature fluctuations in the electronmicroscopic image seems to be of the same kind as the bright border around the spot which is attributed to some temperature induced decontamination stimulating the secondary electron emission. This seems to be the first image of the outrunning surface wave, the existence of which was proved by calorimetric measurements [14].

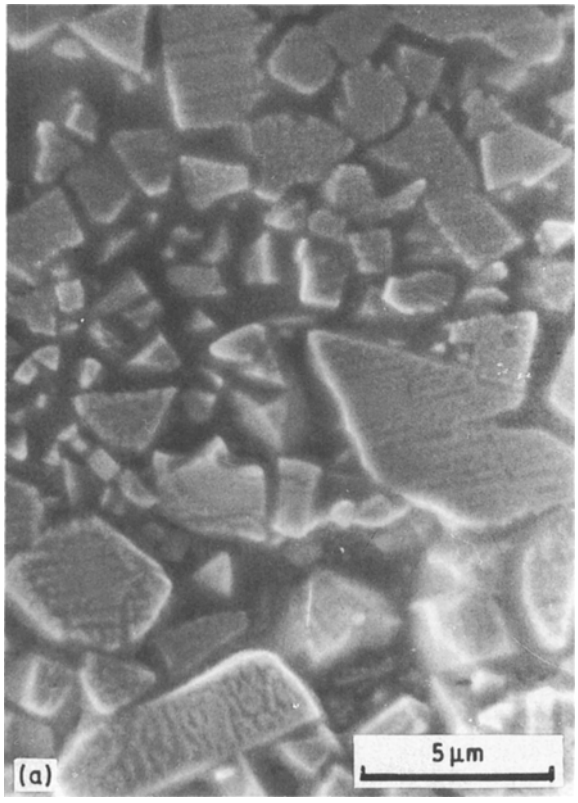

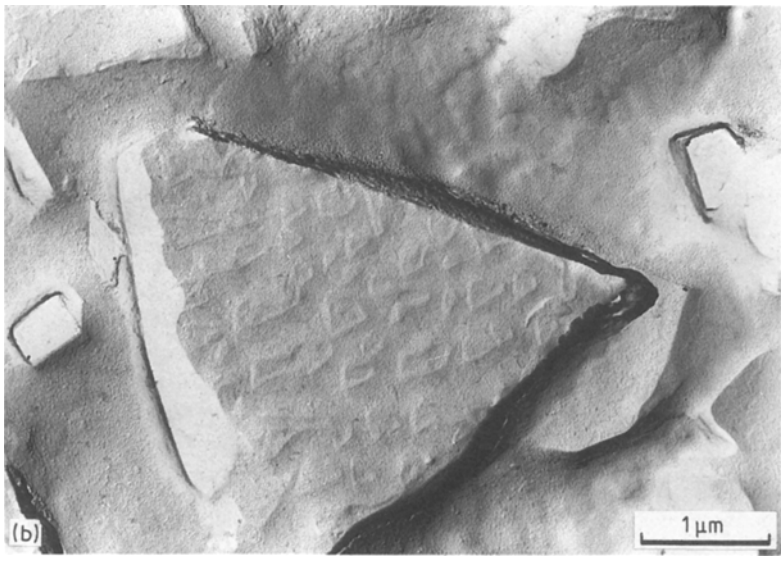

Figure 5 (a) SEM and (b) TEM-replica micrograph showing the fine dispersed precipitates of secondary carbides.

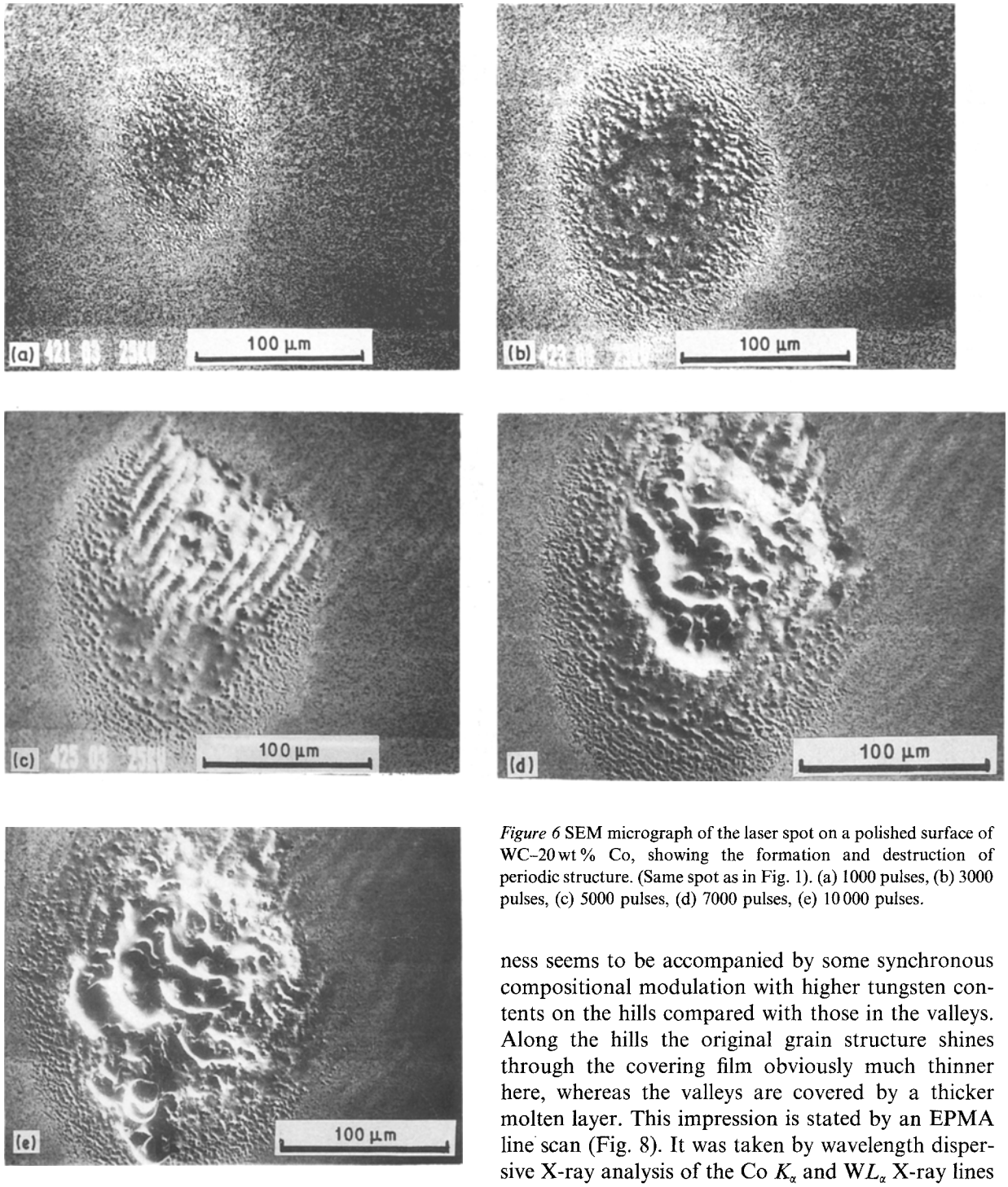

Figure 6 SEM micrograph of the laser spot on a polished surface of WC–20 wt % Co, showing the formation and destruction of periodic structure. (Same spot as in Fig. 1). (a) 1000 pulses, (b) 3000 pulses, (c) 5000 pulses, (d) 7000 pulses, (e) 10 000 pulses.

In order to clarify the nature of the periodic structure and the mechanism for its self-stimulating formation the laser irradiation was stopped, when this structure had been generated and several investigation techniques were employed. A rough impression of both the element distribution and the surface relief is given by backscattered electron (BSE) images using two detectors (A, B). Figure 7b represents the compositional image contrast (A + B) and Fig. 7c the topographic one (A − B) in comparison with the usual secondary electron (SE) image (Fig. 7a).

The latter picture shows clearly that the periodic structure consists of a set of parallel hills and valleys. Brighter appearance in the A + B image (apart from some edge effects) refers to an increased fraction of elements with larger atomic number [15], in our case to a raised tungsten concentration. The periodic waviness seems to be accompanied by some synchronous compositional modulation with higher tungsten contents on the hills compared with those in the valleys. Along the hills the original grain structure shines through the covering film obviously much thinner here, whereas the valleys are covered by a thicker molten layer. This impression is stated by an EPMA line scan (Fig. 8). It was taken by wavelength dispersive X-ray analysis of the Co K_α and WL_α X-ray lines across the periodical structure. The following conclusions can be drawn:

1. Inside the spot cobalt shows clearly a periodical distribution with higher cobalt content in the valleys.
2. Beside the periodical distribution the mean cobalt content is lower inside the laser irradiated area than at the untreated area. The course shows a minimum in the spot centre at which the expected cobalt peak is absent corresponding to a high evaporation rate caused by the temperature maximum.
3. In correspondence to the mean behaviour of cobalt the tungsten content reaches a maximum value in the spot centre.
4. A strong periodical local distribution of tungsten is not observed. This is caused by the superposition of the signals from both WC grains (predominant at the hills) and tungsten solved in cobalt (prevalent in the valleys). Therefore, the clear anticorrelation of

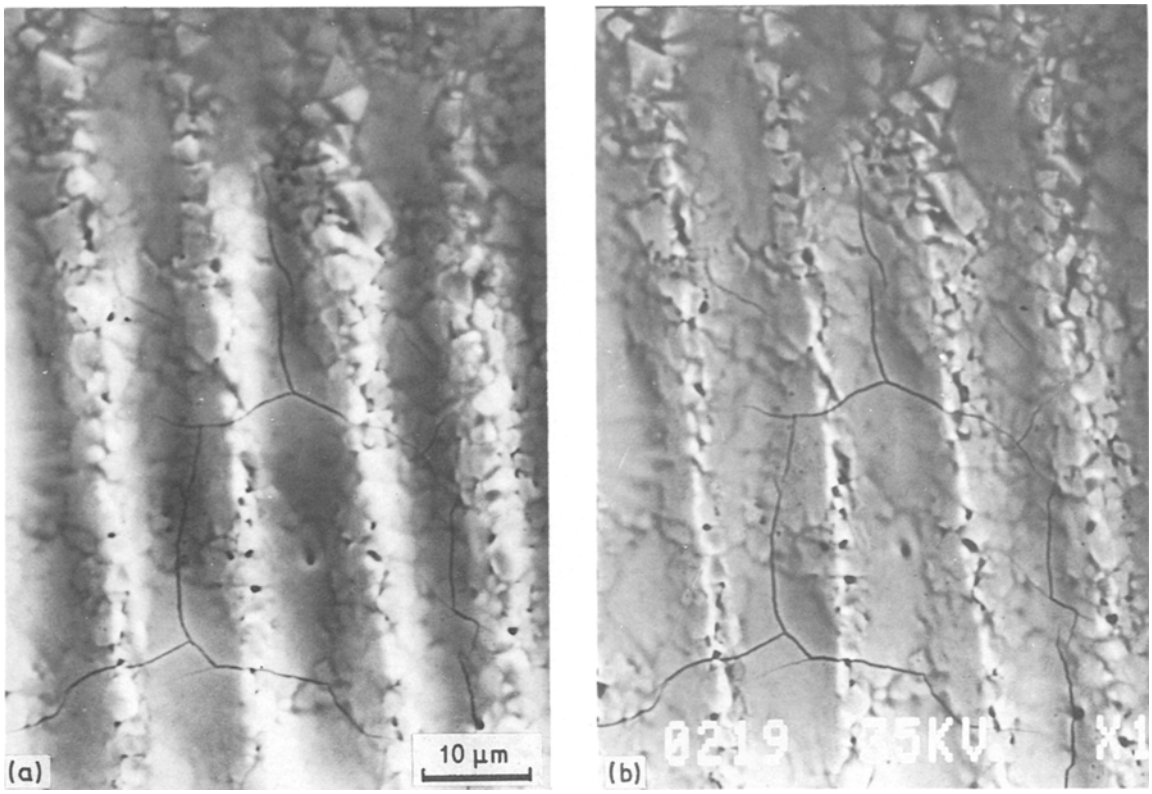

Figure 7 Analysis of a laser spot on a polished surface of WC–20 wt % Co, taken with different SEM methods. (a) Image with secondary electrons (SE); (b), (c) Image with backscattered electrons (BSE). Use of two detectors (A, B) allows separation of (b) compositional contrast (A + B) and (c) topographic contrast (A − B).

tungsten and cobalt signals is not found in the spot in contrary to the outer untreated region.

Additional information including subsurface structure can be gained by means of the ion-beam cutting technique mentioned above (Fig. 9). The sharp section produced in this way shows that the modulated surface profile lies under the level of the original one, i.e. the ripple structure is engraved into the material. The heterogeneous structure characterized by the polygonal carbide grains is destroyed up to distances below the surface much smaller than the wave amplitude of about 4 μm. This invariance proves that any essential contribution of viscoplastic flow can be excluded. These facts are consistent with the concept of temperature-modulated evaporation from the melt as decisive step in ripple formation. The fluctuating thickness of the melt layer should be produced by the competing effects of cobalt evaporation on the top side and carbide dissolution on the underside. Obviously this equilibrium is displaced towards evaporation along the less heated hills leading to the very thin film there, which hardly covers the protruding carbide grains. There may be an additional effect by the usual degradation of surface tension with increasing temperature stimulating the melt to concentrate within the more heated zones.

5. Conclusions

Summarizing the experimental results and their discussion given above, the following conclusions can be drawn:

1. The laser-induced structural modification of cemented carbides is carried out by the melting binder phase. The carbide grains do not directly melt, but are dissolved by the liquid binder, changing the cobalt-rich melt into a tungsten-rich one.

2. Due to the tungsten enrichment of the liquid phase, by self-quenching after irradiation the molten material is transformed to an oversaturated solid solution with fine carbide precipitates.

3. With increasing pulse number the dissolution

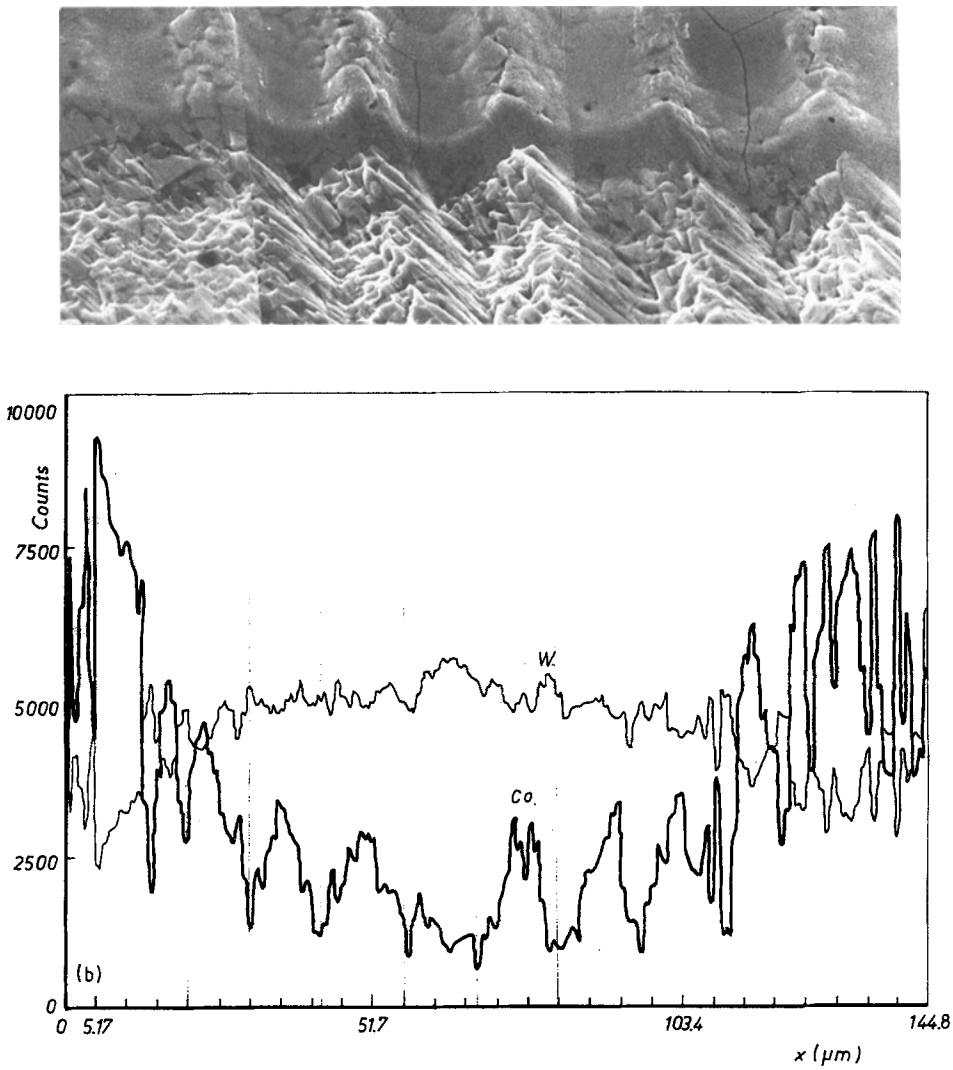

Figure 8 EPMA-line scan through a regularly modulated laser spot, showing the correlation between composition and geometry of the surface.

process is intensified by the rising fraction of highly dispersed secondary carbides. This seems to be connected with an enlarged absorption and correspondingly enlarged energy input.

4. At higher pulse numbers significant material loss by evaporation occurs. Due to resonance amplification of surface modulation, a periodic structure strictly correlated with polarization direction and wave length is thus engraved into the surface.

5. The periodic structure becomes unstable at

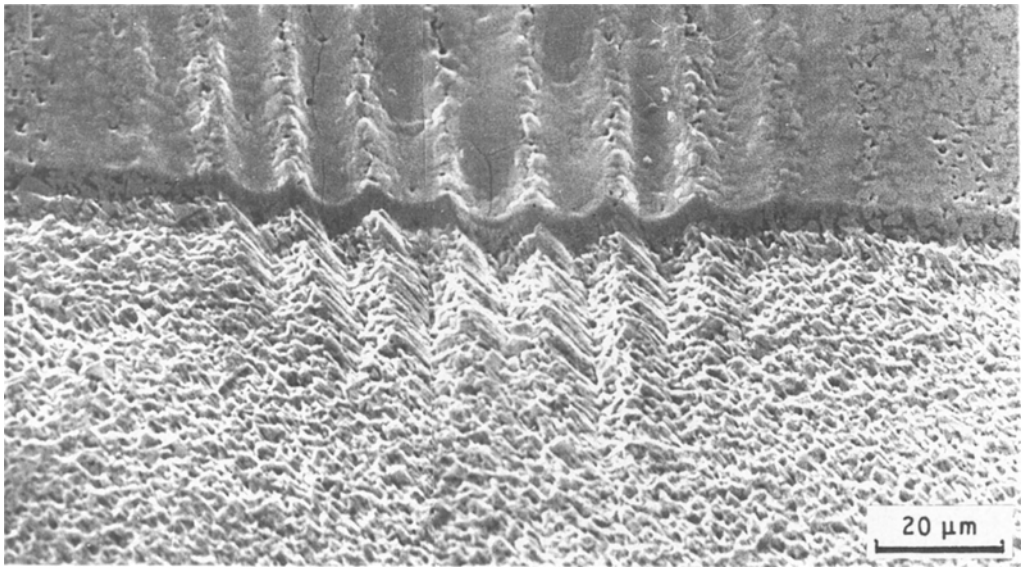

Figure 9 Section through a laser spot with periodic surface modulation. For sectioning (see also Fig. 8) the ion beam slope cutting technique was applied [16].

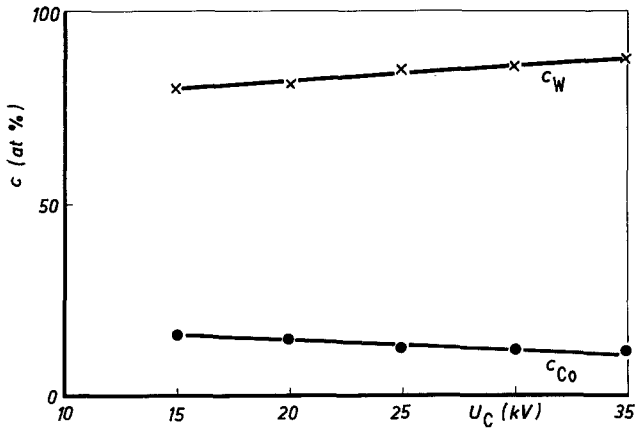

Figure 10 Composition of melt layer in the valleys according to EPMA signals obtained with different acceleration voltages.

continued irradiation when dissolution and lateral viscous flow compensate the local evaporation losses.

References

1. H. MÜLLER, K. WETZIG, B. SCHULTRICH, S. M. PIMENOV, N. I. CHAPLIEV, V. I. KONOV and A. M. PROCHOROV, *J. Mater. Sci.* **24** (1989) 3328.
2. G. LEITNER, B. SCHULTRICH and H. KUBSCH, "Sintering behavour of TiC–Mo_2–C–Ni and WC–Co hard metals" Proceedings of the 7th International Conference on Powder Metallurgy, CSSR, ČSVTS, Ostrava 1979.
3. W. HAUFFE, Thesis B, Technical University Dresden, 1978.
4. W. HAUFFE and B. SCHULTRICH, *Praktische Metallographie* **25** (1988) 517.
5. P. RAUTALA and T. NORTON, 1. Plansee Seminar, Reutte, 1952, p. 303.
6. G. WIRWARK and G. L. DUNLOP, in "Science of Hard Materials", edited by R. K. Viswanadham, D. J. Rowcliffe and J. Gurland (Plenum Press, New York, 1983) p. 311.
7. H. E. EXNER and H. FISCHMEISTER, *Archiv f. Eisenhüttenwesen* **37** (1966) 416.
8. C. WAGNER, *Z. f. Elektrochemic* **65** (1961) 581.
9. H. MÜLLER, A. SEIDLER, J. EDELMANN, K. WETZIG and B. SCHULTRICH, 12th National Conference on Electronmicroscopy, Dresden, 1988, Vol. 2, p. 323.
10. M. J. BIRNBAUM, *J. Appl. Phys.* **36** (1965) 3688.
11. S. A. ACHMANOV, V. I. EMELJANOV, N. I. KOROTEEV and V. N. SEMINOGOV, *Uspechi fiziceskich nauk* **147** (1985) 675.
12. V. I. KONOV and V. N. TOKAREV, *Preprint IOFAN 70*, Moscow, 1985.
13. I. URSU, I. N. MIHAILESCU, A. M. PROKHOROV, V. N. TOKAREV and V. I. KONOV, *J. Appl. Phys.* **61** (1987) 2445.
14. I. URSU, M. DIMESCU, P. M. MIHAILESCU, A. M. PROKHOROV, V. I. KONOV and V. N. TOKAREV, *Phys. Lett.* **2** (1986) 685.
15. L. REIMER, G. PFEFFERKORN, "Rasterelectronenmikroskopie (Springer-Verlag, Berlin 1973).
16. W. HAUFFE (Technical University Dresden, GDR), unpublished results (1988).

Received 24 August 1988
and accepted 12 January 1989